Chemical Engineering Science 313 (2025) 121709

Contents lists available at ScienceDirect

Chemical Engineering Science

journal homepage: www.elsevier.com/locate/ces

Analysis of integrated calcium looping alternatives in a cement plant

Ana Amorim [a,b], Rui M. Filipe [b,c,*], Henrique A. Matos [b]

[a] c5Lab – Sustainable Construction Materials Association, 2795-242 Linda-a-Velha, Portugal
[b] CERENA, Instituto Superior Técnico, Universidade de Lisboa, 1049-001 Lisbon, Portugal
[c] Instituto Superior de Engenharia de Lisboa, Instituto Politécnico de Lisboa, 1959-007 Lisbon, Portugal

ARTICLE INFO

Keywords:
Cement plant model
CO_2 capture
Calcium looping
Integrated configuration
Tail–end configuration

ABSTRACT

Calcium looping is a promising post-combustion CO_2 capturing technology, highly compatible with the cement industry, one of the major industrial sources of CO_2 emissions. Limestone, a raw material for clinker, forms lime, a calcium looping adsorbent. Thus, it is possible to maximize the synergies between a cement plant and a calcium looping unit by establishing an integrated configuration. Nevertheless, the integration of calcium looping in cement plants has not yet been thoroughly studied. This study examines different integration alternatives, developing models for the preheater and calciner using Aspen Plus, validated with operational data, alongside an entrained-flow carbonator model considering adsorbent deactivation. By combining these models, six integrated configurations are proposed and compared with the tail–end calcium looping configuration. The integrated configurations show a reduction in fuel consumption and net energy consumption for the same CO_2 avoided emissions. The most promising configuration was identified and a comparative techno-economic analysis was conducted.

1. Introduction

Approximately 36 Gton of CO_2 were emitted into the atmosphere worldwide in 2021, and these emissions are still rising. The cement industry's contribution to the CO_2 global emissions has been increasing in the past years and it reached 7–8 % of the total emissions, making it the second major industrial source of CO_2 emissions, after the iron and steel sector (Our World in Data, 2021).

Calcium looping is a carbon capture technology based on the reaction between CO_2 and calcium oxide (CaO), whose implementation in cement plants offers synergies, since limestone, a raw material for cement production, is also used as an adsorbent in the calcium looping process. It is possible to further increase the synergies between a cement plant and a calcium looping capturing unit by establishing an integrated configuration, instead of a tail-end configuration. Initially proposed by Romano et al. (2014), the integrated configuration requires that the calciner of the capturing process is included in the cement plant by replacing the existent calciner. Thus, the calciner serves a dual–purpose of regenerating the calcium–based adsorbent and calcining the raw meal before it enters the rotary kiln. Although difficult to retrofit into existing cement plants due to its lower flexibility, the integrated configuration has advantages in terms of fuel consumption and direct CO_2 emissions reduction (De Lena et al., 2019). The Buzzi Unicem Vernasca pilot plant was built as part of the CLEANKER project in Italy to study integrated calcium looping (Fantini et al., 2021).

The particle size of the raw meal in the cement plant, which corresponds to the particle size of the adsorbent in the integrated calcium looping, is in the range of 10 to 20 μm (Spinelli et al., 2018). Thus, these particles may fall into Geldart Group C ($d_p < 30\mu m$), which is the most difficult group to fluidize, since the particles tend to have a cohesive behaviour and experience channelling (Cocco et al., 2014). Circulating fluidized bed reactors are the most studied reactors for the calcium looping process, since they provide high solid circulation rates and excellent gas–solid contact heat transfer, easing heat and mass transfer. However, given the difficulty of the particle to fluidize, entrained-flow reactors were proposed as an alternative for the integrated configuration (Knowlton, 2013). A recent study was carried out by De Lena et al. (2022) on using circulating fluidized beds in the integrated configuration. The particle size of the limestone in the preheater of their proposed configuration was in the range of 100 to 200 μm and the fragmentation occurring in the calciner would decrease the particle size to the size required by the kiln. However, this configuration requires more significant changes in the preheater and experimental testing it at a relevant scale. Therefore, the use of entrained-flow reactors operating under a dilute pneumatic transport regime was considered a more suitable

* Corresponding author.
E-mail address: rfilipe@isel.ipl.pt (R.M. Filipe).

https://doi.org/10.1016/j.ces.2025.121709
Received 6 December 2024; Received in revised form 18 March 2025; Accepted 18 April 2025
Available online 20 April 2025

Nomenclature

Abbreviations Acronyms

BEC	Bare Erected Cost
CAPEX	Capital Expenditure
CEPCI	Chemical Engineering Plant Cost Index
CFD	Computational Fluid Dynamics
$C_{indirect}$	Indirect Costs
CPU	Compression and Purification Unit
EC	Equipment Cost
HT	High Throughput
IC	Installation Cost
IR	Infrared Absorption
LOI	Loss on Ignition
OC	Owner's Cost
OPEX	Operational Cost
SRC	Steam Rankine Cycle
TCD	Thermal Conductivity
TDC	Total Direct Cost
TGA	Thermogravimetric Analysis
TPC	Total Plant Cost
XRF	X-Ray Fluorescence

Chemical compounds

C_2S	$(CaO)_2{\cdot}(SiO_2)$
C_3A	$(CaO)_3{\cdot}(Al_2O_3)$
C_3S	$(CaO)_3{\cdot}(SiO_2)$
C_4AF	$(CaO)_4{\cdot}(Al_2O_3){\cdot}(Fe_2O_3)$

Nomenclature

C_{CO_2}	CO_2 concentration in the gas phase, mol•m^{-3}
$C_{CO_2,eq}$	Equilibrium CO_2 concentration in the gas phase, mol•m^{-3}
d_p	Particle diameter, m
E_a	Activation energy of the carbonation reaction, J•mol^{-1}
f_{calc}	Calcination level, –
f_{carb}, f_{carb}'	Carbonation level, –
F_0	Fresh adsorbent molar flowrate, mol•s^{-1}
F_{CaO_i}	Calcium oxide molar flowrate entering the carbonator, mol•s^{-1}
F_R	Adsorbent molar flowrate cycling from calciner to carbonator, mol•s^{-1}
h	Thickness of the product layer of an adsorbent particle, m
k	Deactivation constant of an adsorbent particle, –
k_0	First-order carbonation kinetic constant, mol•m^{-2}•s^{-1}•Pa^{-1}
k_r	First-order carbonation kinetic constant, m^3•mol^{-1}•s^{-1}
k_s	Intrinsic kinetic constant of the carbonation reaction, m^4•mol^{-1}•s^{-1}
N	Number of carbonation/calcination cycles, –
N_{age}	Number of complete carbonation/calcination cycles, –
$p_{CO_2,eq}$	Equilibrium partial pressure of CO_2, Pa
r_{CO_2}	Carbonation reaction rate, mol•m^{-3}•s^{-1}
$r_{N_{age}}$	Fraction of particles with N_{age} complete carbonation/calcination cycles, –
R	Universal gas constant, J•mol^{-1}•K^{-1}
S_N	Specific surface area available for carbonation in the particle, m^2•m^{-3}
t	Time, s
T	Temperature, K
V	Volume, m^3
$V_{M,CaCO_3}$	Molar volume of $CaCO_3$, m^3•mol^{-1}
$V_{M,CaO}$	Molar volume of CaO, m^3•mol^{-1}
V_R	Volume of the carbonator, m^3
X	Carbonation conversion, –
$X_{max,N_{age}}$	Maximum conversion for particles with N_{age} complete carbonation/calcination cycles, –
$X_{max,ave}$	Averaged maximum carbonation conversion, –
X_r	Adsorbent residual conversion, –

Greek letters

τ	Residence time in the carbonator, s

option for this configuration.

Spinelli et al. (2018) proposed a 1D fluid dynamic model for an entrained-flow carbonator for integrated calcium looping. As reviewed by Hanak et al. (2015), the adsorbents undergoing calcium looping deactivate over multiple carbonation/calcination cycles. Romano (2012) proposed a circulating fluidized bed carbonator model for the tail-end calcium looping that, unlike the model proposed by Spinelli et al. (2018) for the integrated calcium looping, includes the deactivation of the adsorbent and the influence of a fresh adsorbent stream on the average adsorbent conversion and carbon capture efficiency.

One of the main goals of this work is to propose an alternative method for modelling the entrained-flow carbonator reactor and compare the results with the ones obtained by Spinelli et al. (2018). To obtain the maximum conversion as a function of the raw meal and recycled absorbent flowrates in the carbonator, the deactivation of the adsorbent is included in the carbonator model proposed in this work.

On the other hand, the integration of the calcium looping in the cement plant has not been fully studied yet. The initial configuration proposed by Romano et al. (2014) considers the carbonator receiving the gas directly from the cement plant rotary kiln, which increases the cooling duty in this piece of equipment and the fuel consumption when compared to the other configuration proposed in the literature (De Lena et al., 2019). In the alternative configuration, the kiln gas is cooled by heating the raw meal in a 2-cyclone preheater, which increases the energy efficiency of the process. The effect of further changing the cyclone preheater arrangement in the integrated calcium looping scheme on the performance of the calcium looping is not addressed in the literature. Therefore, this work also focuses on the comparison of integrated calcium looping configurations, to obtain an improved alternative in terms of energy consumption, using the carbonator model proposed in this paper and data from a Portuguese cement plant as a case study.

2. Models

2.1. The cement plant case study

The case study considered a cement plant producing approximately 120 ton/h of clinker and presenting the configuration shown in Fig. 1. In this cement plant, the raw meal is fed to the top cyclone of a 5-cyclone preheater. The solid materials are heated in the preheater and reach a calciner, in which fuel is provided for their calcination before entering the rotary kiln. The gas released at high temperature in both the kiln and the calciner is sent to the preheater to heat the raw meal in counter–current.

The preheater and calciner of a cement plant were modelled using Aspen Plus. The Aspen Plus model is represented in Appendix A of the supplementary materials. The raw meal and flue gas data were provided by an industrial partner, and it is presented in Table 1 and Table 2, respectively. The fuels used and their respective characterisation, heating value and relative percentage of use are presented in Table 3.

The clinker constituents, C_2S, C_3S, C_3A and C_4AF, are not fully characterised in the Aspen Plus database. Thus, it was necessary to

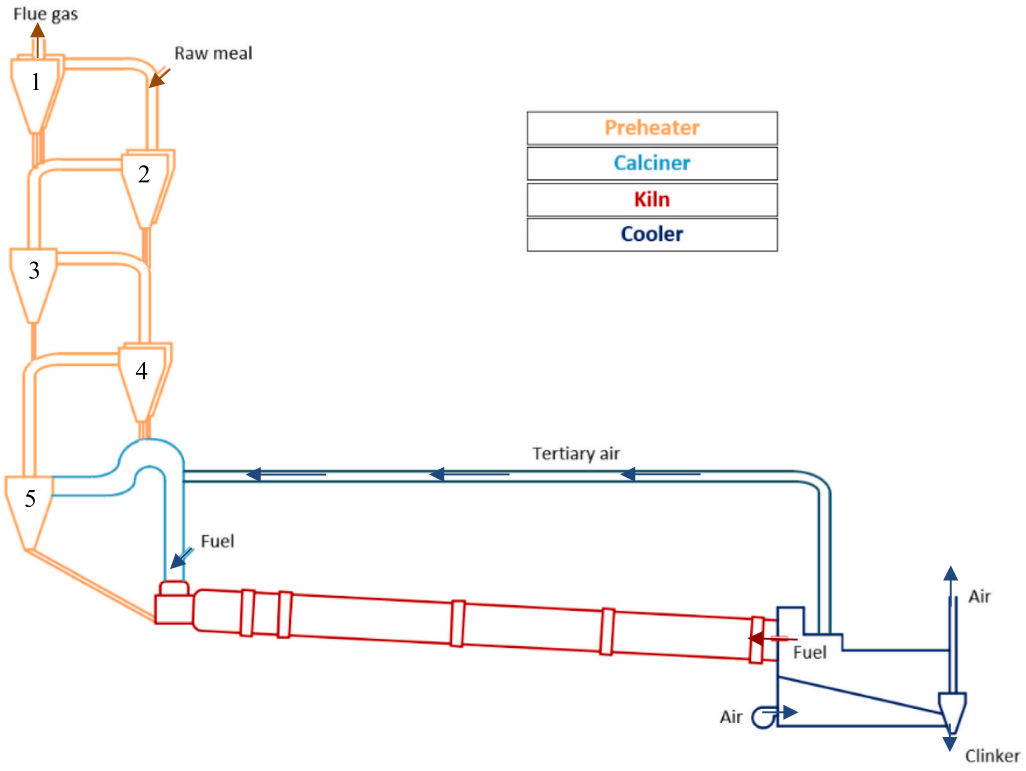

Fig. 1. Basic schematic configuration of a cement plant.

Table 1
Raw meal characterisation based on data provided by an industrial partner.

		Composition (wt%)	Method
Compounds	SiO_2	13.02	XRF
	Al_2O_3	03.74	
	Fe_2O_3	02.14	
	CaO	44.17	
	MgO	01.08	
	LOI	35.85	TGA (110 °C – 950 °C)
Particle size (μm)	0–45	67.4	Sieving
	45–63	7.7	
	63–90	8.3	
	90–212	14	
	212–315	1.9	
	315–630	0.7	

LOI: Loss on ignition; XRF: X-ray fluorescence; TGA: Thermogravimetric analysis.

Table 2
Outlet gas components based on data provided by an industrial partner.

Flue gas component	Composition (%)
N_2	64.97
O_2	3.23
CO_2	31.33
CO	0.47

provide further information, such as the free energy of formation and the enthalpy of formation. These values were obtained from Lothenbach et al. (2008) and are presented in Table 4.

The raw meal stream input was determined based on chemical analysis performed on the material before entering the preheater. Each cyclone of the preheater was modelled as a set of two units, a Gibbs reactor model, which minimizes the free energy of Gibbs and determines the most stable compounds at the reactor temperature, and a cyclone to separate the solid and gas streams. The cyclones were modelled in simulation mode and their diameter was determined based on the pressure drop data of each cyclone. The cyclone efficiency was calculated based on the model by Dietz (1981) and the inlet design of the cyclone was considered as being a spiral with high throughput – swift-HT. This model and inlet design were chosen, as it was the one which led to lower deviations from the operational data. This model divides the cyclone into three regions and considers the effect of turbulence and particle fluxes. As the diameter of the cyclones is higher than 1.5 m, a high throughput (HT) cyclone was considered. Given the lack of kinetic data and residence time in the cyclones, the chemical equilibrium approach was used. However, chemical equilibrium is not easily achieved in cyclones since the reactions do not occur instantly. Therefore, in this work, an equilibrium reactor model was used at an apparent temperature below the real one to simulate the actual industrial data, whose reaction extension is smaller than the equilibrium obtained with the real temperature. This calculated apparent temperature is different for each cyclone and was estimated by minimizing the difference between the model and the real industrial data. False air, which consists of ambient air infiltrations into the process, is reported by the industrial partner to enter the preheater. Based on the flowrates of nitrogen and oxygen in each stream of the preheater, it was determined the false air would enter the preheater mainly in the first cyclone. As such, it was considered a stream of false air entering this piece of equipment.

The total heat loss in the preheater by radiation and convection was approximately 120 $kJ \bullet kg_{clinker}^{-1}$, according to the information provided by an industrial partner. This value is in line with the radiation and convection heat losses reported by other authors (Kabir et al., 2010; Khalifa & Alsadig, 2019; Verma et al., 2020). The heat loss in each cyclone was estimated proportionally to the amount of heat exchanged in the cyclone.

A calciner was also considered in the model, having as an input three

Table 3
Calciner fuel characterisation based on data provided by an industrial partner.

		Petroleum coke	Automotive shredder residue	Shredded tyres	Method
Proximate analysis (%)	Moisture	00.6	01.0	00.6	TGA
	Fixed carbon	80.2	06.1	21.5	Calculation
	Volatile Matter	13.2	67.7	58.5	TGA
	Ash	6.6	26.2	20.0	TGA
Elemental analysis (%)	Carbon	82.16	59.51	71.55	IR
	Hydrogen	03.54	07.37	06.52	IR
	Nitrogen	01.81	00.90	00.25	TCD
	Chlorine	00.01	01.84	00.05	Potentiometry
	Sulphur	05.13	00.43	01.32	IR
	Oxygen	00.75	03.75	00.31	Calculation
Particle size (μm)	0–45	79.9	0.2	0.0	Sieving
	45–63	12.9	0.1	0.0	
	63–90	5.0	0.1	0.0	
	90–212	1.9	0.1	0.0	
	212–315	0.3	3.9	0.0	
	315–630	0.0	0.9	0.0	
	315–1250	0.0	1.0	0.0	
	1250–2500	0.0	1.4	0.0	
	2500–5000	0.0	2.0	0.0	
	5000–10000	0.0	6.4	0.0	
	10000–20000	0.0	28.9	0.9	
	20000–40000	0.0	55.0	10.1	
	> 40,000	0.0	0	89.0	
Heating value (kcal•kg^{-1})		7803	6512	7368	Calorimetry
Calciner feed (wt%)		34	37	29	–

TGA: Thermogravimetric analysis; TCD: Thermal conductivity; IR: Infrared absorption

Table 4
Standard enthalpy and free energy of formation at 25 °C (Lothenbach et al., 2008).

Compound	$\Delta_f G^o$ (kJ•mol^{-1})	$\Delta_f H^o$ (kJ•mol^{-1})
C_3S	−2784.33	−2931
C_2S	−2193.21	−2308
C_3A	−3382.35	−3561
C_4AF	−4786.50	−5080

different fuels, petroleum coke, shredded tyres, and automotive shredder residue. The combustion simulation of these non–conventional compounds in the calciner was based on the recommendations of the Aspen Plus 8.4 manual AspenTech (2013). This is a two-step approach, in which the first step is the decomposition into gas molecules (N_2, O_2, S, H_2, H_2O, Cl_2) and solids (C, Ash) and the following step is the minimization of the free energy of Gibbs with the addition of the heat released in the decomposition step. A tertiary air stream, which comes from the clinker cooler, is fed to the calciner, allowing the fuels' combustion. According to the data provided by the industrial partner, there are heat losses by radiation and convection of around 30 kJ•kg$^{-1}_{clinker}$ in the tertiary air duct. A heat exchanger was included in the model to simulate the cooling of the tertiary air flow. The products from the calciner were mixed with the gas stream from the cement kiln and sent to the fifth cyclone, whose solid product enters the cement kiln.

2.2. Tail-end calcium looping

The standard implementation of calcium looping carbon capture is the tail–end calcium looping, i.e. an end–of-pipe process only treating the gas effluent from the cement process (the "Flue gas" stream shown in Fig. 1). A schematic representation of this technology is presented in Fig. 2. The Aspen Plus model of the tail–end calcium looping configuration is represented in Appendix A of the supplementary materials. To estimate the CO_2 capture efficiency, an input variable of the Aspen Plus model, the carbonator model proposed by Romano (2012) is used. The model is implemented in Python language and includes the adsorbent deactivation over successive carbonation/calcination cycles. The experimental deactivation data obtained by Marques et al. (2023) was fitted to Equation (1), as proposed by Grasa & Abanades (2006) and used in the model to simulate adsorbent deactivation. In this equation, $X_{max,N}$ corresponds to the maximum conversion of the adsorbent, N to the number of carbonation/calcination cycles, X_r to the adsorbent residual conversion and k to the deactivation constant. Based on the region where the limestones were extracted, their chemical composition and porosity varies leading to distinct adsorption behaviours. Therefore, the results were grouped into two categories according to the adsorbent conversion, type H and type L, corresponding to adsorbents with higher or lower maximum carbonation conversion, respectively. The fitting of the results is shown in Fig. 3. Both X_r and k are fitting parameters, which take the values 0.2 and 1.6, respectively, for the higher conversion adsorbents group and 0.04 and 5.6, respectively, for the lower conversion adsorbents group. The process model was build taking the higher conversion adsorbent group fitting parameters.

$$X_{max,N} = \frac{1}{1/(1+X_r)+kN} + X_r \tag{1}$$

The average maximum conversion, $X_{max,ave}$, is the sum of the products between the fraction of particles undergoing N_{age} complete carbonation/calcination cycles, $r_{N_{age}}$, and the respective conversion for that fraction of particles, $X_{max,N_{age}}$, as presented in Equation (2). $r_{N_{age}}$ is calculated using Equation (3), proposed by Rodríguez et al. (2010), in which F_0 is the fresh sorbent molar flowrate, F_R is the recycled sorbent molar flowrate, N_{age} is the number of complete carbonation-calcination cycles, f_{carb} is the carbonation level, which is the ratio between the average carbonation conversion and the maximum average carbonation conversion, and f_{carc} is the calcination level, the ratio between the average calcination conversion and the maximum average calcination conversion. The average carbonation conversion was determined following the procedure described by Romano (2012). It was assumed the maximum calcination conversion was reached, which corresponds to a f_{carb} of 1.

$$X_{max,ave} = \sum_{N_{age}=1}^{+\infty} X_{max,N_{age}} \cdot r_{N_{age}} \tag{2}$$

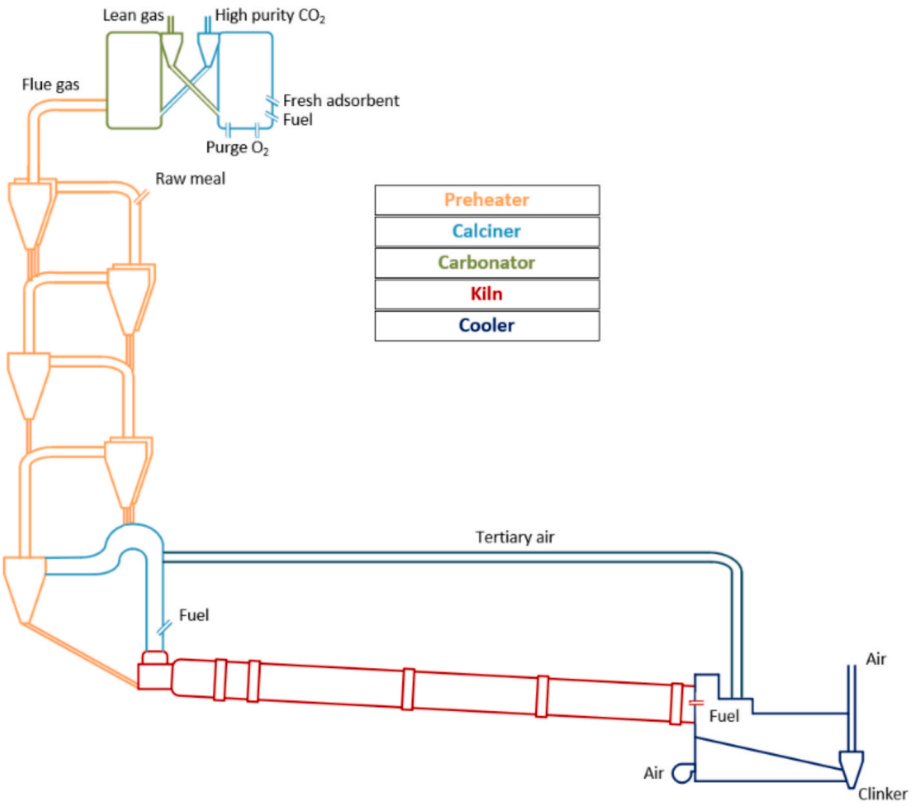

Fig. 2. Schematic representation of the tail-end calcium looping configuration in a cement plant.

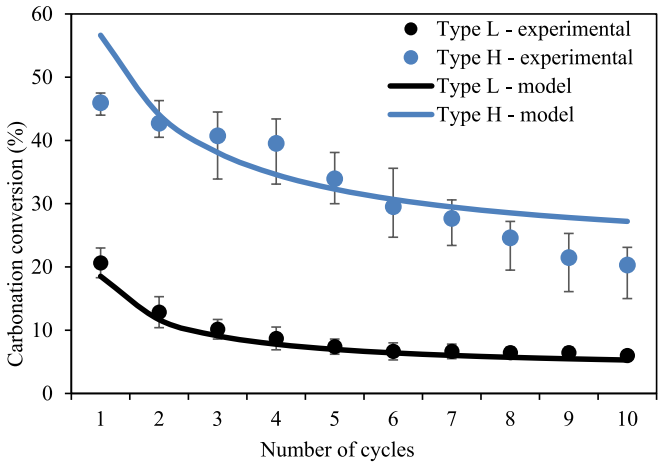

Fig. 3. Adsorbent deactivation obtained by Marques et al. (2023) for two different categories, type H and type L adsorbents, and fitted by the semi-empirical equation proposed by Grasa & Abanades (2006).

$$r_{N_{age}} = \frac{\left[\frac{F_0(1-f_{calc})}{F_0+F_R f_{calc}} + \frac{F_0}{F_R}\right] f_{carb}^{N_{age}-1} f_{calc}^{N_{age}}}{\left(\frac{F_0}{F_R} + f_{carb} f_{calc}\right)^{N_{age}}} \quad (3)$$

The carbonator and calciner temperatures were set to 700 °C and 930 °C, respectively, to mimic the experimental conditions for which the deactivation curves were obtained. The calciner fuels, petroleum coke, shredded tyres, and automotive shredder residue, were also used in the calcium looping unit and their amount was calculated proportionally to the fuel input in the cement plant case study to maintain the calciner temperature at 930 °C. However, the combustion of these materials was performed under oxyfuel conditions, with an oxygen excess of 4 %, to obtain a high purity stream leaving the calciner. After leaving the calciner, the gas stream is compressed and purified in a compression and purification unit (CPU).

A ratio of recycled adsorbent molar flowrate to inlet CO_2 molar flowrate (F_R/F_{CO2}) of 4 and a ratio of fresh adsorbent molar flowrate to inlet CO_2 molar flowrate (F_0/F_{CO2}) of 0.07 were used. These conditions led to the maximum CO_2 capture efficiency at this temperature, 91.3 % (Amorim, 2024).

A steam Rankine cycle (SRC) was included in the model to produce electricity. The maximum steam pressure was selected as 100 bar, similar to what was considered by De Lena et al. (2017). The fluid removing heat from the carbonator should not change its physical state. Therefore, a recycling stream, H2O–6 (Supplementary materials), was added to maintain the inlet stream of the carbonator, H2O–4, in the gas form. The total electric energy produced in the turbine was maximized by varying the flowrate of water in the cycle, the outlet pressure of the turbine and the split ratio of S-2, while maintaining the temperature of the H2O–5 stream at a maximum of 680 °C and both H2O-4 and the turbine outlet H2O-8 streams in the vapor phase.

2.3. The carbonator of the integrated configuration

The carbonator of the integrated configuration was modelled as an entrained-flow reactor, based on the Aspen Plus reactor model for plug flow. A representation of this model is shown in the Supplementary Materials (Appendix A). The developed model was compared with the model proposed by Spinelli et al. (2018). Three scenarios considered by Spinelli et al. (2018), with different percentages of recirculated adsorbent in the reactor (Table 5), were used for model validation. Spinelli et al. (2018) do not report the composition of the gas except for the CO_2 content. The stream in our model was assumed to be composed of CO_2, H_2O, N_2 and O_2, and its composition was calculated considering the stream density given by Spinelli et al. (2018), and an N_2 to O_2 ratio of

Table 5
Model assumptions for validating the carbonator model (Spinelli et al., 2018). Cases 1, 2 and 3 correspond to cases 16, 17 and 18 presented by Spinelli et al. (2018), respectively.

Gas flowrate	
Mass ($kg \bullet s^{-1}$)	17.06
Volume ($Nm^3 \bullet s^{-1}$)	12.44
Gas composition (vol%)	
CO_2	19.8
N_2	55.2
H_2O	10.3
O_2	14.7
Solid flowrate from calciner ($kg \bullet s^{-1}$)	62.2
Solid composition (wt%)	
CaO	65.5
$CaCO_3$	00.2
SiO_2	21.6
Al_2O_3	5.0
Fe_2O_3	002.7
MgO	02.4
$CaSO_4$	02.6
Adsorbent	
Maximum conversion (%)	20
Particle size (μm)	30
Carbonator solids recirculation (%)	
Case 1	0
Case 2	50
Case 3	66.7
Carbonator reactor	
Inlet temperature (°C)	600
Length (m)	60
Diameter (m)	3.6

79:21.

The carbonation reaction kinetics was defined after Grasa & Abanades (2006) by Equation (4). This first–order kinetics was also assumed by Romano (2012) for the carbonator model of the tail–end calcium looping. As shown in Equation (4), the kinetic rate is calculated as a function of the specific surface area available for reaction in a particle after experiencing N carbonation/calcination cycles, S_N, which in turn is given by the maximum adsorbent conversion after N carbonation/calcination cycles, $X_{max,N}$, multiplied by the ratio between the $CaCO_3$ and CaO molar volumes and divided by the thickness of the product ($CaCO_3$) layer in the particle, h (Equation (5)). Unlike the model by Romano (2012), which assumed isothermal operation, the model proposed in this work considers an adiabatic reactor. The temperature plays an important role and the variation of the kinetic constant with temperature was considered. The kinetic constant, k_r, is a first order kinetic constant based on concentration. Therefore, k_r can be calculated based on the constants obtained by Sun et al. (2008), using Equation (6). Aspen Plus requires the kinetics to be inserted in the form of concentration rate instead of conversion rate, given as a function of the reactants' concentration. Thus, the equation was reformulated based on the plug flow reactor model, as presented in Equation (7). The final carbonation reaction considered is given by Equation (8). The differential variation of the volume with time was assumed uniform and it was approximated by the ratio between the reactor volume and the residence time.

$$\frac{dX}{dt} = k_r\left(C_{CO_2} - C_{CO_2,eq}\right) = k_s S_N (1-X)^{2/3}\left(C_{CO_2} - C_{CO_2,eq}\right) \tag{4}$$

$$S_N = \frac{V_{M,CaCO_3} X_{max,N}}{V_{M,CaO} h} \tag{5}$$

$$k_r = k_0 e^{-E_a/RT} RT (1-X)^{2/3} \frac{V_{M,CaCO_3} X_{max,N}}{h} \tag{6}$$

$$-r_{CO_2} = -\frac{dC_{CO_2}}{dt} = F_{CaO_i}\frac{dX}{dV} = F_{CaO_i}\frac{dX}{dt}\frac{dt}{dV} \tag{7}$$

$$-\frac{dC_{CO_2}}{dt} = F_{CaO_i} k_0 e^{-E_a/RT} RT (1-X)^{2/3} \frac{V_{M,CaCO_3} X_{max,N}}{h} C_{CO_2} \frac{\tau}{V_R} \tag{8}$$

As carbonation is an equilibrium reaction, an equilibrium concentration, $C_{CO_2,eq}$, must be considered, as given by Equation (4). However, the direct inclusion of this equilibrium concentration in the kinetic expression as it is represented in Equation (4) is not possible using Aspen Plus, because the kinetic expression cannot include subtracting terms. Thus, to account for the subtracting term based on the CO_2 equilibrium concentration, the reverse reaction, calcination, was considered a zero–-order reaction under the form presented in Equation (9). The equilibrium partial pressure of CO_2, $p_{CO_2,eq}$, was calculated using the regression obtained by Barin (1989), presented in Equation (10).

$$\frac{dC_{CO_2}}{dt} = F_{CaO_i} k_0 e^{-E_a/RT} (1-X)^{2/3} \frac{V_{M,CaCO_3} X_{max,N}}{h} p_{CO_2,eq} \frac{\tau}{V_R} \tag{9}$$

$$p_{CO_2,eq} = 4.137 \times 10^{12} e^{-\frac{20474}{T}} \tag{10}$$

The parameters used in the calculation of the CO_2 concentration along the reactor are presented in Table 6.

The temperature and the solid conversion were calculated along the reactor. As the residence time depends on the carbonation kinetics, temperature and flowrates, a design specification was created in the Aspen Plus model to achieve convergence between the residence time calculated by the model and the residence time taken as an input for the kinetic model.

When internal recirculation is considered, the inlet flowrate of CaO, F_{CaO_i}, will vary depending on the extension of the reaction. Thus, a design specification was also considered in this case to reach convergence between the inlet calcined adsorbent flowrate and the one considered in the kinetics calculation.

2.4. Adsorbent deactivation

The model developed by Spinelli et al. (2018), which was used for comparison with the proposed model, did not consider the adsorbent deactivation, taking 20 % as the maximum adsorbent conversion, regardless of the fresh-to-recycled adsorbent ratio.

In the cement plant preheater, each cyclone has two inlet streams as shown in Fig. 1, one solid stream from the upward cyclone and one gas stream from the downward cyclone. The solid flowrate entrained in the gas stream is lower than the solid flowrate in the inlet solid stream. Therefore, it was assumed that 100 % of the CaO and $CaCO_3$ arriving at the calciner were fresh adsorbent (F_0), although the solid flowrate entrained in the gas stream can contain recirculated adsorbent. The recycled adsorbent (F_R) was calculated as the sum of the CaO and $CaCO_3$ flowrates leaving the carbonator and entering the calciner. The calculation of the maximum average adsorbent conversion is made using the algorithm presented in Fig. 4, implemented as an Aspen plus calculator block. The carbonation level, f_{carb}', is calculated through Equation (11)

Table 6
Parameters used for the calculation of the CO_2 concentration along the entrained-flow reactor.

Parameter	Value	Reference
$k_0(mol \bullet m^{-2} \bullet s^{-1} \bullet Pa^{-1})$	1.67×10^{-7}	Sun et al. (2008)
$E_a(J \bullet mol^{-1})$	2.9×10^4	Sun et al. (2008)
$V_{M,CaCO_3}(m^3 \bullet mol^{-1})$	36.9×10^{-6}	Romano, (2012)
h(m)	50×10^{-9}	Alvarez & Abanades, (2005)

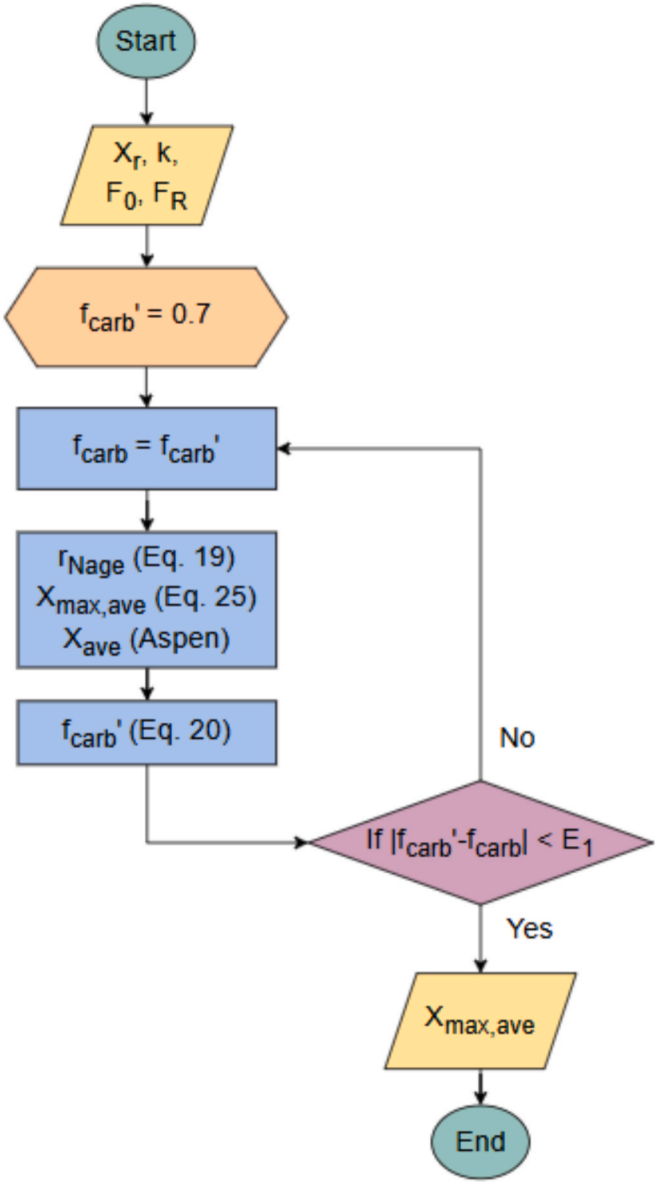

Fig. 4. The algorithm inserted in the Aspen Plus calculator block to obtain the maximum average carbonation conversion. X_r is the residual conversion, k the deactivation constant, f_{carb} (or f_{carb}') the carbonation level, r_{Nage} the fraction of solids with N_{age} cycles of carbonation calcination cycles, $X_{max,\ ave}$ the average maximum carbonation conversion, X_{ave} the average carbonation conversion (imported from the Aspen Plus simulation) and F_0 and F_R are the fresh calcium oxide and the recirculated calcium oxide molar flowrates, respectively. The error E1 was set to 10^{-3}.

and the difference between the consecutive calculated values is used as the stop criteria of this algorithm. X_{ave} corresponds to the average conversion, which is obtained considering the extent of the reaction calculated in the Aspen model.

$$f_{carb}' = \frac{X_{ave}}{X_{max,ave}} \tag{11}$$

2.5. Integrated configurations

Only one integrated calcium looping configuration is considered in recent studies and no comparison of other possible integrated calcium looping configurations is presented in the literature. Therefore, in this work, six different configurations to integrate the calcium looping unit and the cement preheater are proposed (Fig. 5) and compared. The differences and similarities among the configurations are represented in a schematic process diagram in Fig. 6. To allow the comparison with the tail-end calcium looping configuration, the same CO_2 avoided emissions were considered.

Configuration I is based on the one proposed by De Lena et al. (2019), with two different entries of raw meal in the system and with the material exiting the calciner going directly to the kiln. However, in the configuration proposed by De Lena et al. (2019), the cooling of the carbonator internal recirculation is performed by the cooled tertiary air and lean gas streams. In this work, it is proposed to remove the heat generated in the carbonator through the cooling of the adsorbent recycled stream using direct steam and producing superheated steam. This decreases the number of heat exchangers needed and it is expected to reduce the size of the adsorbent cooler due to the higher isobaric specific heat of steam when compared to air. Furthermore, laboratory studies show a positive impact of steam addition on the carbonation kinetics and in reducing the adsorbent deactivation (Arcenegui Troya et al., 2022; Dong et al., 2020). Nevertheless, the effect of steam in the carbonation conversion was not considered in this study, which leads to conservative results.

Configurations II and III were based on configuration I, but with a different cyclone distribution above and below the calciner. On the other hand, configurations IV to VI only consider one raw meal inlet and the calcined raw meal passing through the last cyclone of the preheater before entering the rotary kiln. The integrated configurations are comparatively characterised in Table 7. The cyclone preheater is divided into the CO_2 preheater and the kiln preheater, depending on the gas stream circulating in these cyclones. The CO_2 preheater corresponds to a group of cyclones, whose gas stream is the concentrated CO_2 stream, and the kiln preheater is the part of the preheater whose gas stream is the kiln gas before capture.

For all the configurations, the flowrate of the raw meal, with the same composition as in the case study, was varied to maintain the flowrate of solids fed to the kiln. The design of the cyclones on the preheater in the integrated configuration was considered the same as in the cement plant preheater model. However, in all the integrated configurations, a cyclone has been added at the top of the preheater to reduce raw meal losses in the flue gas and maintain raw meal requirements similar to the cement plants. The diameter of the additional cyclone was determined so that its efficiency decreases the material loss in the outlet gas of the preheater to the value of a cement plant without capture.

These integrated calcium looping configurations were compared with the tail-end calcium looping in terms of fuel consumption, electricity production and CO_2 outlet purity. The CO_2 avoided emissions of the integrated configuration were set to be the value obtained for the tail-end calcium looping. This was achieved by changing the internal recirculation of the carbonator and allowing the comparison of the different configurations.

As in the tail-end configuration, the combustion in the calciner was performed with an excess of 4 % oxygen and the fuel input was changed to maintain the calciner temperature at 930 °C, which is the temperature reported for the experimental deactivation provided by Marques et al. (2023). While in configurations I to III, the solids reach the kiln at 930 °C (calcination temperature), in configurations IV to VI, the solid stream leaving the calciner is further heated by the gas stream leaving the cement kiln, which leads to an increase of the temperature at the entry of the kiln. This means the energy requirements of the kiln to raise the temperature to 1300–1500 °C will decrease. To compare the configurations in terms of total fuel input, the savings obtained using a higher temperature solid stream were accounted as a reduction in the fuel consumption equivalent to a fictitious cooling of the solid stream to 930 °C, the temperature in configurations I, II and III.

As an example, the Aspen plus model of configuration I is presented in the Supplementary Materials (Appendix A). After leaving the

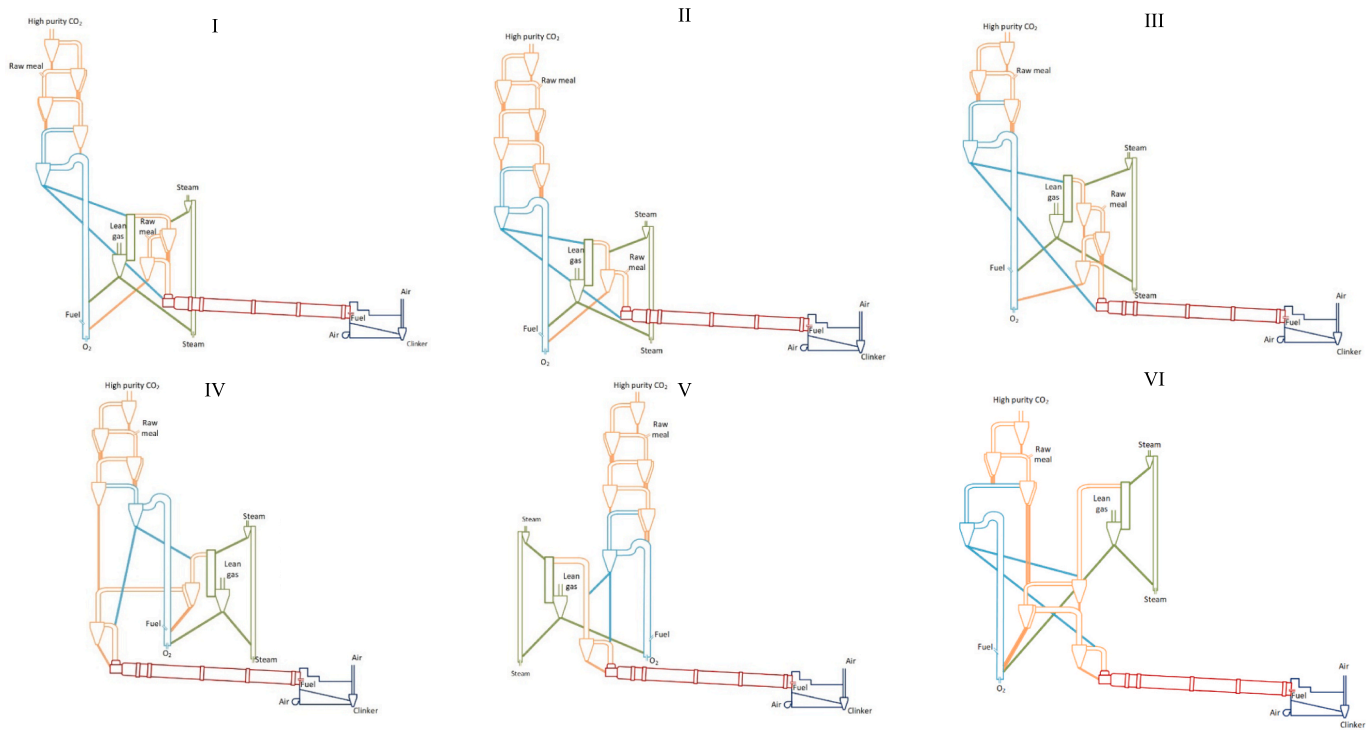

Fig. 5. Calcium looping integrated configurations. The preheater is represented in orange, the carbonator in green, the calciner in light blue, the rotary kiln in red and the clinker cooler in dark blue. The differences among the configurations are the cyclone distribution in the two preheaters, the number of raw meal inlet streams and the route of the calcined material. (For interpretation of the references to colour in this figure legend, the reader is referred to the web version of this article.)

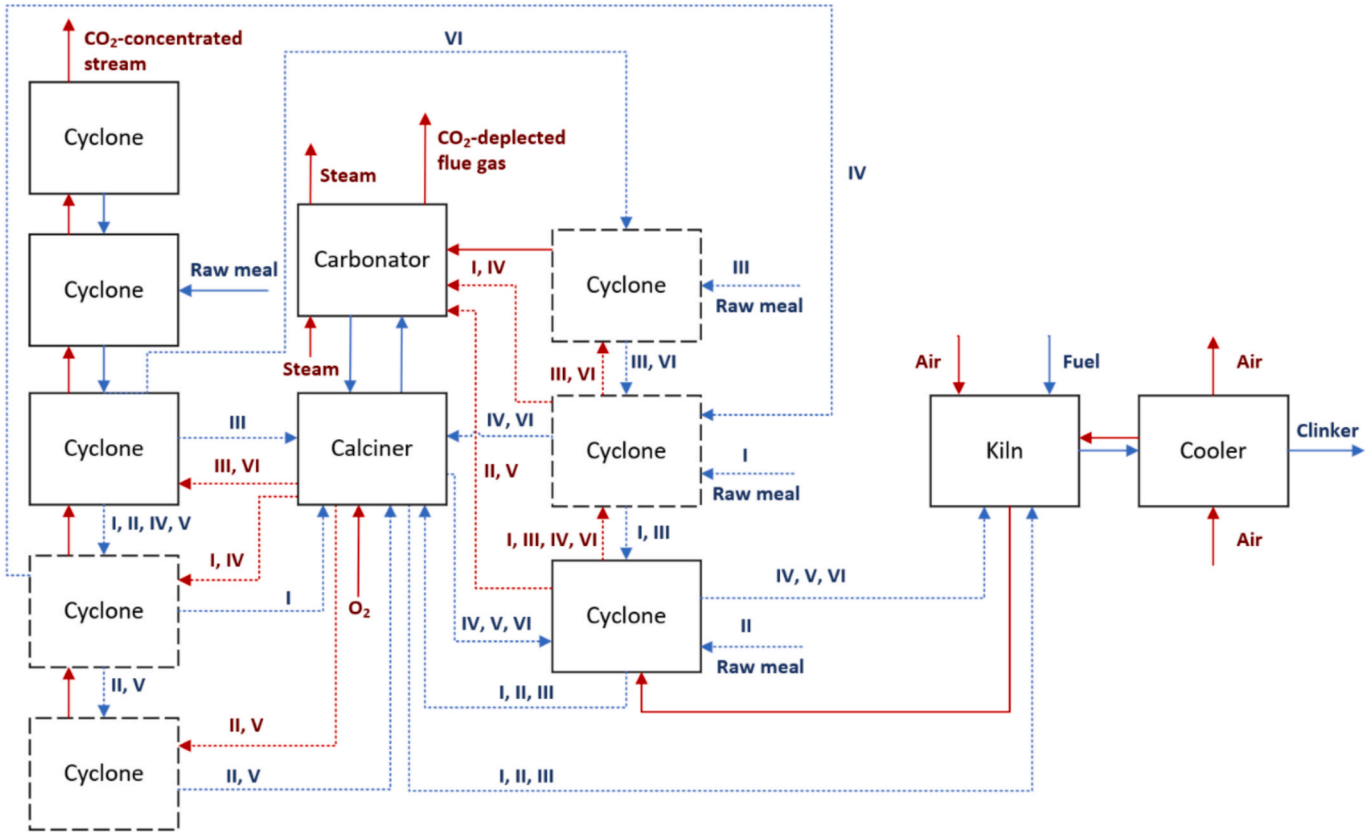

Fig. 6. Superstructure scheme considering the alternative calcium looping integrated configurations. The dashed lines represent alternatives that vary according to the configuration and the straight lines are drawn when no alternative is considered. The configurations which follow the alternative are identified with the correspondent number. The dashed boxes represent equipment that it is not present in all the configurations. The blue lines represent solid streams and the red lines gas streams. (For interpretation of the references to colour in this figure legend, the reader is referred to the web version of this article.)

Table 7
Characterisation of the integrated calcium looping configurations.

	Raw meal inlet streams	Calciner solid stream outlet	Cyclones in the CO_2 preheater	Cyclones in the kiln preheater
Integrated I	2	Carbonator + Kiln	4	2
Integrated II	2	Carbonator + Kiln	5	1
Integrated III	2	Carbonator + Kiln	3	3
Integrated IV	1	Carbonator + Last cyclone	4	2
Integrated V	1	Carbonator + Last cyclone	5	1
Integrated VI	1	Carbonator + Last cyclone	3	3

additional cyclone, the gas ("High purity CO_2" stream) is further treated in a two-stage CPU with intermediate water removal, as in the tail-end configuration. A steam cycle was also applied for energy recovery in the six schemes of the integrated calcium looping. This steam cycle recovers heat from the lean gas, the concentrated CO_2, the tertiary air streams of the cement plant, and the recirculated adsorbent cooler. The electricity production in the turbine was maximized by varying the water flowrate in the steam cycle, the recycling stream flowrate, and the turbine outlet pressure, while maintaining the outlet stream of the turbine and the cooler heat removing fluid in the vapour phase. The Aspen plus models of the CPU and the steam cycle are represented in the Supplementay materials (Appendix A).

2.6. Techno-economic analysis

After modelling all the calcium looping sections, an economic analysis was conducted to compare alternatives. The units were planned to work continuously for 8000 h per year. The equipment cost was estimated based on the correlations presented in Table 8. The cost obtained for each piece of equipment (EC) was updated to 2023 using the CEPCI values, by Equation (12).

Table 8
Estimation of the equipment costs, *EC*[M€], for the tail-end calcium looping units. CFB is circulating fluidized bed reactor and EF is entrained-flow reactor.

Equipment	Cost estimate	Reference
CFB Carbonator	$EC = 7.5 \cdot \left(\frac{F_{in}}{55.35}\right)^{0.67}$	Gardarsdottir et al. (2019); Voldsund et al. (2019)
CFB Calciner	$EC = 5.3 \times 10^2 \cdot \left(\frac{Q_{calc}}{164.6}\right)^{0.67}$	Gardarsdottir et al. (2019); Voldsund et al. (2019)
EF Carbonator	$EC = 85.9 \times 10^{-3} \cdot \dot{V}_{in}^{0.5}$	De Lena et al. (2019)
EF Calciner	$EC = 52.5 \times 10^{-3} \cdot \dot{V}_{out}^{0.5}$	De Lena et al. (2019)
Solid cooler / Additional cyclone	$EC = 3.98 \times 10^{-9} D_{cyc}^2 + 2.73 \times 10^{-6} D_{cyc} + 1.6 \times 10^{-2}$	De Lena et al. (2019)
CPU	Compressors, Heat exchangers, Separators	Matches' Equipment Cost Estimates, (2014); Aspen Capital Cost Estimator®, (n.d.)
Steam cycle	Pump, Turbine, Condenser, Evaporators	Aspen Plus®; Equipment Costs for Plant Design and Economics for Chemical Engineers - 5th Edition, (2011); Matches' Equipment Cost Estimates, (2014)

Q_{calc}– Heat required in the calciner [MW_{th}]; D_{cyc} – cyclone diameter ($1548 \cdot \dot{V}^{0.28}$) [mm]; $\dot{V}$– volumetric flowrate in the cyclone [m^3/s]; F_{in} – Inlet gas flowrate of the CFB carbonator; $\dot{V}_{in}$ – Inlet gas flowrate of the EF carbonator [m^3/s]; $\dot{V}_{out}$ – Outlet gas flowrate of the EF calciner [m^3/s].

$$Cost_{2023} = \frac{CEPCI_{2023} \cdot Cost_{year}}{CEPCI_{year}} \quad (12)$$

The capital expenditure (CAPEX) was calculated as the sum of the total plant cost (TPC) of the cement plant and capture unit, using Equations (12) to (16) and with the assumptions presented in Table 9 (Gardarsdottir et al., 2019). In these equations, BEC is the bare erected cost, EC is the equipment cost, IC is the installation cost, TDC is the total direct cost, OC is the owner's cost, $C_{indirect}$ is the indirect costs and TPC is the total plant cost.

$$BEC = \sum_{Equipment=i} EC_i + IC_i \quad (13)$$

$$TDC = BEC + Contingencies_{process} \quad (14)$$

$$TPC = TDC + Contingencies_{project} + OC + C_{indirect} \quad (15)$$

$$CAPEX = TPC_{Cementplant} + TPC_{captureunit} \quad (16)$$

The assumptions used in the calculation of the operational expenditure are presented in Table 10.

3. Results and discussion

3.1. The cement plant case study

The relative deviation values between the preheater/calciner simulation and the real cement plant data were calculated based on Equation (17) and are presented in Table 11. Given the lack of industrial operational data regarding the solid flowrates at the exit of the cyclones 2, 3, 4 and 5, it was not possible to calculate their mass flowrate powder deviations.

$$Deviation(\%) = \frac{Calculated - Real}{Real} \times 100 \quad (17)$$

In cyclone 5, the temperature is higher than expected and the temperature in cyclone 1 is lower than expected. This is explained by the assumption that false air (unwanted air which enters the process e.g. through the gaskets) is fully entering into the first cyclone. As the deviations between the data and the model are mainly below 10 %, the model was validated.

The real data (composition and temperature) of the preheater outlet stream is compared in Table 12 with the results given by the model simulation. The concordance between the two enables to continue working with the simulated stream data. Therefore, the simulated preheater outlet stream was used as the inlet stream to be processed in the tail–end calcium looping unit and as base case scenario of a cement plant without carbon capture.

3.2. The carbonator of the integrated configuration

To address the integration of the calcium looping unit in the cement plant case study, an entrained–flow reactor model was developed in this

Table 9
Calculation of the parcels to estimate the capital expenditure.

Parcel	Calculation
IC_i	25 % EC_i
$Contingencies_{process}(Integrated)$	72 % *BEC*
$Contingencies_{process}(Tail-end)$	32 % *BEC*
$Contingencies_{project}$	15 % *TDC*
OC	7 % *TDC*
$C_{indirect}$	14 % *TDC*

Table 10
Assumptions in the calculation of the operational expenditure.

Category	Parcels	Cost
Utilities	Raw meal	3.01 €/ton
	Petroleum coke	3.68 €/GJ
	Alternatives	0.56 €/GJ
	Electricity	58.1 €/MWh
Taxes	Carbon tax	70 €/ton
	Insurance and local tax	2 % TPC
Labour	Operating labour (OL)	40 k€/year/person
	Maintenance labour (ML)	40 % Maintenance cost
	Administrative and support labour	30 % (OL + ML)
Other costs	Maintenance cost	2.5 % TPC
	Other cement plant costs	0.8 €/ton cement

A sensitivity analysis was performed to the carbon tax (0–150 €/ton), electricity price (± 50 %), fuel price (± 50 %) and CAPEX variations (± 30 %).

Table 11
Deviations of the preheater model results in comparison with real cement plant operational data.

Process variables deviations (%)	Cyclone 1	Cyclone 2	Cyclone 3	Cyclone 4	Cyclone 5
Mass flowrate powder	8.5	–	–	–	–
CO_2 composition in the gas	−5.0	−0.6	−2.4	1.8	−5.6
N_2 composition in the gas	1.6	3.5	3.0	4.6	1.6
O_2 composition in the gas	4.9	−8.6	0.3	−19.6	−8.5
Temperature	−8.7	0	0	0	8.1
Gas volumetric flowrate	−4.1	−2.0	2.4	2.2	6.5

Table 12
Characterisation of the outlet stream of the preheater. Results obtained from the model and the industrial partner operational data.

	Case study model	Real data
Temperature (°C)	294	322
H_2O (%)	2.8	–
N_2 (%)	65.9	65.1
O_2 (%)	3.5	3.2
CO (%)	0.0	0.5
CO_2 (%)	30.6	31.3
Particles (wt%)	10.8	10.4

work. The results obtained using this entrained–flow carbonator model were compared with the results obtained by Spinelli et al. (2018). This comparison is presented in Table 13 for 3 cases of a downflow reactor presented in Spinelli et al. (2018). The deviations between the developed model and the one in the literature are below 10 %. Therefore, this model was considered a valid alternative to the model proposed by Spinelli et al. (2018) and it was used for the simulation of the six integrated calcium looping configurations.

3.3. Configurations comparison

Six integrated configurations, which include the cement plant case study, and the carbonator model validated in the last sections, were modelled and compared with each other and with the tail-end calcium looping configuration in terms of key performance parameters, such as the CO_2 concentrated outlet stream purity and the energy efficiency. Information regarding the estimated temperatures in each configuration can be found in the Supplementary material.

As previously mentioned in subchapter 2.5, an additional cyclone was added to the preheater in the integrated configurations to decrease material losses in the outlet gas stream. The diameter of such cyclone was calculated to maintain the same material losses reported for the plant without capture. On the other hand, the raw meal flowrate was changed to obtain a similar flowrate of material reaching the cement kiln. Both the cyclone diameter and the ratio between the raw meal needed in each configuration and the raw meal required in the cement plant without capture are presented in Table 14 for each integrated calcium looping configuration. The two raw meal inlet streams in configurations I, II and III result in a higher number of fines reaching the carbonator, which leads to higher particle content in the lean gas leaving the carbonator. Thus, the raw meal requirements to maintain the kiln feed flowrate increase for these configurations. As the total raw meal inlet is divided in configurations I, II and III, although the total raw meal inlet is higher in these configurations, the flowrate of solids in the outlet gas stream is lower, which leads to lower efficiency requirements in the extra cyclone to perform the stream separation. Thus, the diameter of the extra cyclone in configurations I, II and III is higher than in the analogous 1-raw meal entry configuration (configurations IV, V and VI, respectively).

Electric energy production depends on the implemented steam

Table 14
Required dimensions of the cyclone at the top of the preheater to maintain the material loss of the cement plant without capture and ratio between the inlet raw meal of the integrated configurations and the cement plant raw meal (raw meal ratio) to obtain the same flowrate of material fed to the kiln.

Configuration	Extra cyclone diameter (m)	Raw meal ratio
Integrated I	2.4	1.1
Integrated II	2.2	1.1
Integrated III	2.9	1.1
Integrated IV	2.2	1.0
Integrated V	1.9	1.0
Integrated VI	2.6	1.0

Table 13
Comparison of the results obtained using the carbonator model developed in this work and the model by Spinelli et al. (2018).

	Case 1[a] Spinelli et al. (2018)	This work	Deviation (%)	Case 2[b] Spinelli et al. (2018)	This work	Deviation (%)	Case 3[c] Spinelli et al. (2018)	This work	Deviation (%)
Recirculation (%)	0	0	–	50	50	–	66.7	66.7	–
Solid/gas ratio at reactor inlet ($kg \bullet Nm^{-3}$)	5	5	0.0	10.29*	10.21	00.8	15.67	15.39	1.8
CO_2 capture efficiency (%)	56.2	61.3	9.1	81.4	81.9	00.6	90.1	90.6	0.6
Outlet temperature (°C)	753.0	730.6	3.0	709.3	697.2	01.7	680.3	678.9	0.2
Adsorbent conversion (%)	8.6	9.3	8.1	12.5	12.4	00.8	13.8	13.7	0.7
Reaction heat ($MJ \bullet kg^{-1}$)	11.0	11.8	7.3	16.0	15.8	01.3	17.7	17.5	1.1

* The value was modified from the Spinelli et al. (2018) reported value to close the mass balance.
[a] Corresponds to case 16 in Spinelli et al. (2018).
[b] Corresponds to case 17 in Spinelli et al. (2018).
[c] Corresponds to case 18 in Spinelli et al. (2018).

Rankine cycle. The optimal water flowrate, turbine outlet pressure and recycling separation ratio which maximizes the electricity production are represented in Table 15. The integrated configurations with the optimized steam cycle were compared with each other and with tail-end calcium looping in terms of i) the capture efficiency needed for obtaining the same CO_2 avoided emissions, ii) CO_2 purity at the preheater outlet, iii) fuel consumption, iv) electric energy produced in a steam cycle, v) net electricity production, and vi) energy efficiency, and the results are presented in Table 16. CO_2 avoided emissions of 91.3 % were defined for all the configurations. For obtaining these avoided emissions, the capturing efficiency (i) in the integrated calcium looping is lower. This value does not correspond to the carbonator capture efficiency because the preheater in the integrated configuration operates under oxyfuel combustion, and its emissions are sent directly to the CO_2 concentrated stream. Therefore, the carbonator only captures the emissions from the kiln, requiring carbonator capture efficiencies in the range 58–71 % for avoiding 91.3 % of the CO_2 emissions of the cement plant.

From Table 16, it is also possible to conclude that the CO_2 concentrated stream purity (ii) obtained in the integrated configurations using the existing cement plant preheater is approximately 78 %, while the purity in the tail-end calcium looping is above 90 %. The low purity of the integrated calcium looping is related to the entrance of the false air in the cyclone preheater. Preheaters with lower leakage and/or with isolation on the entry of the raw meal should be considered to increase the CO_2 concentration of the stream.

On the other hand, as the flowrate of gas treated in the carbonator is lower in the integrated configuration (as only the emissions from the kiln are treated), the adsorbent cycling from the carbonator to the calciner which requires regeneration is lower, which leads to a lower fuel consumption in the calciner. Furthermore, in the integrated configuration, the gas stream does not require heating, unlike the tail-end calcium looping, which further reduces the fuel requirements of the process. The fuel requirements of the process are represented in Table 16 as the ratio between the fuel input in each configuration and the fuel input without capture (iii), which is lower in the integrated configurations. Since the extension of the carbonation reaction is higher in tail-end calcium looping, the electric energy recovered in the steam cycle (iv) is higher, leading to a higher net electricity production (v). However, as the fuel requirements are also higher, the energy efficiency (vi) of the configurations was estimated according to equation (18). By comparing the integrated calcium looping configurations, it is possible to notice the configurations with only one raw meal inlet stream and passing in a cyclone after exiting the cyclone and before entering the kiln (IV, V, VI) present higher energy efficiencies than configurations I, II and III, which have two raw meal inlets and go directly from the calciner to the kiln. From the two sets of integrated configurations, configuration IV and configuration I are the ones which show the highest efficiencies, although presenting the higher fuel consumption. Configurations I and IV have the same cyclone distribution, 4 cyclones in the CO_2 preheater (including the additional cyclone) and 2 cyclones in the kiln preheater. This is an intermediate distribution when compared to the others, which highlights its advantages. Therefore, configuration IV seems the most promising integrated configuration to apply to a cement plant, since it is the one with the highest energy efficiency.

$$Energy\ efficiency = \frac{Net\ energy\ production}{Fuel\ consumption_{with\ capture} - Fuel\ consumption_{without\ capture}} \quad (18)$$

3.4. Techno-economic analysis

A techno-economic analysis was performed to compare the tail-end configuration and the integrated configuration IV, which was the one presenting the highest energy efficiency. The results are shown in Table 17.

Given the lower technology readiness level of integrated calcium looping, the considered contingencies for the integrated configuration were higher (72 % of BEC) than in the tail-end configuration (32 % of BEC). Nevertheless, the estimated capital investment for the integrated configuration was lower. This is mainly due to considering entrained flow reactors for carbonation and calcination, which present lower costs. The operational costs of the integrated configuration were also lower than in the tail-end configuration, mainly due to the low fuel consumption. The cost of avoided CO_2 is lower than the considered carbon tax (70 €/ton), which means the implementation of both the tail-end and the integrated configuration IV are economically feasible.

A sensitivity analysis was performed to the carbon tax, the fuel and electricity prices and CAPEX. The results are presented in Fig. 7. From the sensitivity analysis, it is possible to conclude that variations of 50 % on the price of electricity do not impact the economic viability of the capture units. On the other hand, an increase of 50 % on the fuel price or 30 % on the CAPEX compromise the viability of the tail-end configuration. The implementation of the integrated configuration IV will remain viable with an increase of 50 % on the fuel price or 30 % on the CAPEX. The carbon tax significantly impacts the economic viability of the capture units.

4. Conclusion

In this work, the calcium looping was studied in detail, by comparing six different integrated and one tail–end configurations. In the integrated configurations, variations in the raw meal feed, carbonator and calciner positions in the preheater and rotary kiln feed were considered. As a first step, a cement plant preheater and calciner were modelled using Aspen Plus and the model was validated using real operational data provided by an industrial partner. For establishing an integrated calcium looping configuration, a new entrained-flow carbonator, where the adsorbent deactivation over multiple carbonation and calcination cycles was considered, was also modelled using Aspen Plus. The results obtained with this model were compared with a published CFD model and showed deviations of less than 10 %. Using both the preheater/calciner and the carbonator models, the integrated configurations were built and compared with a tail-end calcium looping configuration. All the integrated configurations required an additional cyclone at the top of the preheater to decrease the raw meal losses in the preheater gas outlet. No modifications in the preheater cyclones' dimensions were made and steam was used for the adsorbent cooling in the carbonator. The integrated calcium looping led to a decrease in fuel consumption and an increase in energy efficiency when compared to a tail-end calcium looping configuration. One of the most promising integrated calcium looping configurations has only one entry of raw meal and the

Table 15
Steam Rankine cycle optimization results.

	Integrated I	Integrated II	Integrated III	Integrated IV	Integrated V	Integrated VI	Tail-end
Water mass flowrate in the cycle (ton/h)	110	109	108	122	113	112	164
Outlet turbine pressure (bar)	0.23	0.23	0.23	0.24	0.22	0.26	0.42
SRC S-2 recycling percentage (%)	71.0	71.2	71.5	68.9	70.5	70.6	70.7
Electricity production (MW)	42.2	41.6	41.0	46.3	43.9	42.1	53.9

Table 16
Comparison of six integrated calcium looping configurations and the tail-end configuration for obtaining 91.3 % CO_2 avoided emissions.

Parameter	Integrated I	Integrated II	Integrated III	Integrated IV	Integrated V	Integrated VI	Tail-end
i) CO_2 capture efficiency in the carbonator (%) [a]	70.7	70.4	70.1	70.6	58.0	64.1	91.3
ii) Concentrated CO_2 purity (%)	78.1	78.1	78.0	77.5	77.3	77.3	92.7
iii) Equivalent fuel consumption ratio	2.82	2.79	2.79	2.88	2.75	2.74	3.9
iv) Electricity production (MW)	42.2	41.6	41.0	46.3	43.9	42.1	53.9
v) Net electricity production (MW)	15.9	15.5	15.0	19.5	18.0	16.4	27.3
vi) Energy efficiency	13.5	13.4	12.9	16.0	15.9	14.6	10.7

[a] Capture efficiency needed in the carbonator to obtain 91.3 % CO_2 avoided emissions. A lower value means the carbonator needs a lower capture efficiency to avoid the same CO_2 emissions to the atmosphere.

Table 17
Cost comparison of the tail-end and integrated configuration with the reference cement plant.

	Cement plant without capture	Plant with Tail-end Configuration	Plant with Integrated Configuration IV
CAPEX (M€)	277	509	490
OPEX (M€/year)	97.4	65.5	58.8
Cost of cement (€/t_{cement})	95.3	89.0	82.4
Cost of avoided CO_2 (€/ton)	–	59.6	48.8

solids leaving the calciner are fed to a cyclone before entering the kiln. For application into a cement plant producing approximately 120 ton/h of clinker, this configuration requires 2.88 times the fuel of a plant without capture. However, it allows the production of 19.5 MW of electric energy, leading to a energy efficiency of 16 % and a CO_2 avoided cost of 48.8 €/ton. For the same CO_2 avoided emissions, the tail-end configuration produces more electric energy, 27.3 MW, but requires 3.9 times the fuel of the cement plant, which leads to lower energy efficiency (10.7 %) and a higher CO_2 avoided cost (59.6 €/ton).

CRediT authorship contribution statement

Ana Amorim: Writing – original draft, Visualization, Validation, Methodology, Investigation, Conceptualization. **Rui M. Filipe:** Writing

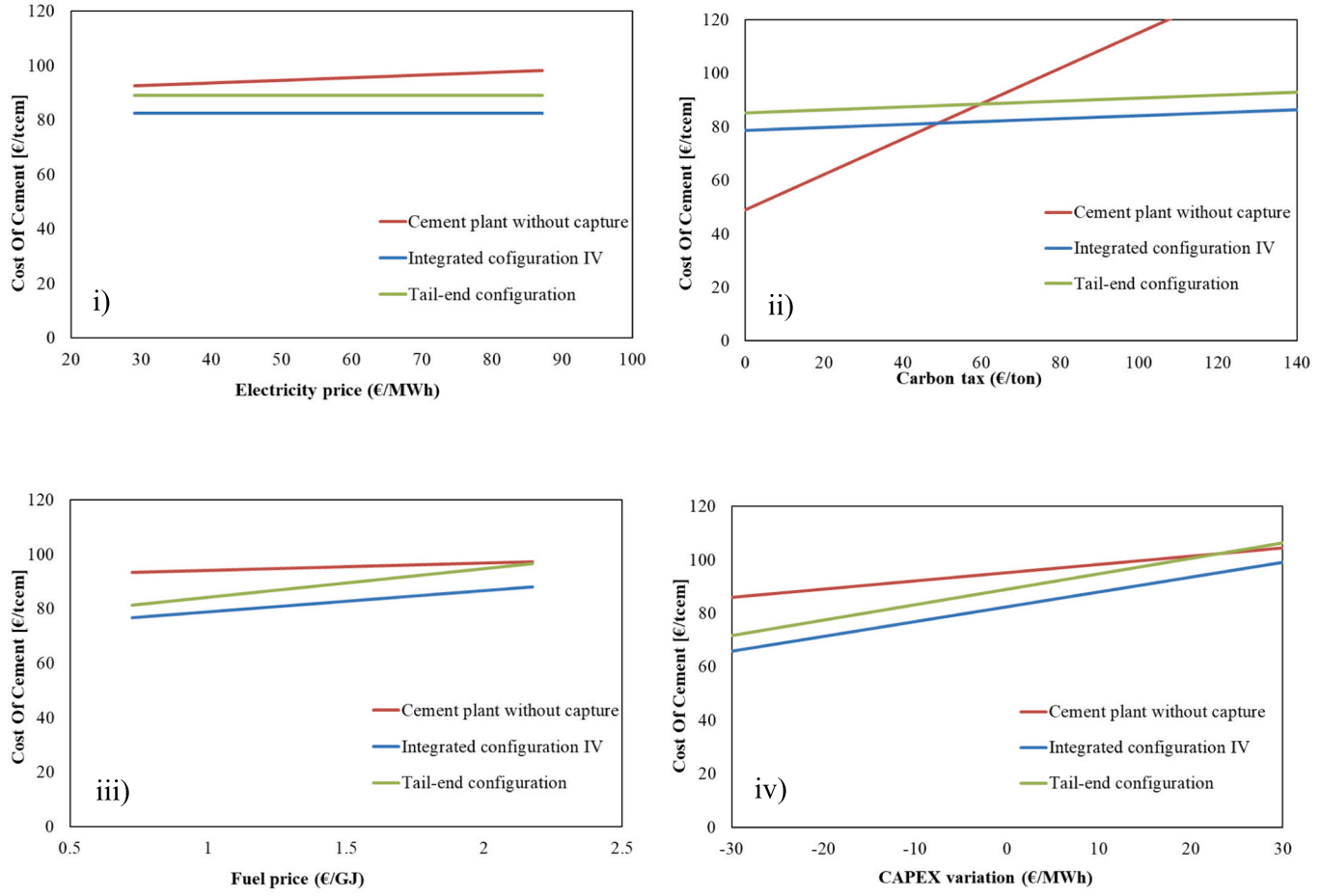

Fig. 7. Comparative sensitivity analysis on the price of electricity (i), carbon tax (ii), fuel price (iii) and CAPEX variation (iv) effect on the cost of cement of the reference cement plant without capture, the integrated configuration IV and the tail–end configuration.

– review & editing, Visualization, Supervision, Conceptualization. **Henrique A. Matos:** Writing – review & editing, Visualization, Supervision, Conceptualization.

Declaration of competing interest

The authors declare that they have no known competing financial interests or personal relationships that could have appeared to influence the work reported in this paper.

Acknowledgements

This work was supported by c^{5}Lab – Sustainable Construction Materials Association [CENTRO-04-3559-FSE-000096; LISBOA-05-3559-FSE-000008; 01/C05-i02/2022] and CERENA [FCT-UIDB/04028/2025 and FCT-UIDP/04028/2025]. The authors also acknowledge Cimpor and Secil for providing real cement plant operational data.

Appendix A. Supplementary data

Supplementary data to this article can be found online at https://doi.org/10.1016/j.ces.2025.121709.

Data availability

Some data is confidential. The rest will be made available on request.

References

Alvarez, D., Abanades, J.C., 2005. Determination of the critical product layer thickness in the reaction of CaO with CO2. *Industrial and Engineering Chemistry Research* 44 (15), 5608–5615. https://doi.org/10.1021/IE050305S/ASSET/IMAGES/LARGE/IE050305SF00008.JPEG.

Amorim, A., 2024. *Modelling and design of the calcium looping process for carbon capture.* Universidade de Lisboa, Instituto Superior Técnico [PhD Thesis].

Arcenegui Troya, J.J., Moreno, V., Sanchez-Jiménez, P.E., Perejón, A., Valverde, J.M., Pérez-Maqueda, L.A., 2022. Effect of Steam Injection during Carbonation on the Multicyclic Performance of Limestone (CaCO3) under Different Calcium Looping Conditions: A Comparative Study. *ACS Sustainable Chemistry & Engineering* 10 (2), 850. https://doi.org/10.1021/ACSSUSCHEMENG.1C06314.

Aspen Capital Cost Estimator®. (n.d.).

AspenTech. (2013). Getting Started Modeling Processes with Solids V8.4. In *Aspen Technology, Inc.*.

Barin, I., 1989. *Thermochemical data of pure substances.* VCH.

Cocco, R., Reddy, S.B., Knowlton, K.T., 2014. Introduction to Fluidization. *American Institute of Chemical Engineers (AIChE)*.

De Lena, E., Arias, B., Romano, M.C., Abanades, J.C., 2022. Integrated Calcium Looping System with Circulating Fluidized Bed Reactors for Low CO2 Emission Cement Plants. *International Journal of Greenhouse Gas Control* 114, 103555. https://doi.org/10.1016/J.IJGGC.2021.103555.

De Lena, E., Spinelli, M., Gatti, M., Scaccabarozzi, R., Campanari, S., Consonni, S., Cinti, G., Romano, M.C., 2019. Techno-economic analysis of calcium looping processes for low CO2 emission cement plants. *International Journal of Greenhouse Gas Control* 82 (January), 244–260. https://doi.org/10.1016/j.ijggc.2019.01.005.

De Lena, E., Spinelli, M., Martínez, I., Gatti, M., Scaccabarozzi, R., Cinti, G., Romano, M. C., 2017. Process integration study of tail-end Ca-Looping process for CO2 capture in cement plants. *International Journal of Greenhouse Gas Control* 67 (November), 71–92. https://doi.org/10.1016/j.ijggc.2017.10.005.

Dietz, P.W., 1981. Collection efficiency of cyclone separators. *AIChE Journal* 27 (6), 888–892. https://doi.org/10.1002/AIC.690270603.

Dong, J., Tang, Y., Nzihou, A., Weiss-Hortala, E., 2020. Effect of steam addition during carbonation, calcination or hydration on re-activation of CaO sorbent for CO2 capture. *Journal of CO2 Utilization* 39, 101167. https://doi.org/10.1016/J.JCOU.2020.101167.

Equipment Costs for Plant Design and Economics for Chemical Engineers. (2011). http://www.mhhe.com/engcs/chemical/peters/data/.

Fantini, M., Balocco, M., Buzzi, L., Canonico, F., Consonni, S., Cremona, R., Gatti, M., Hammerich, J., Koehler, R., Magli, F., Romano, M.C., Spinelli, M., 2021. Calcium Looping Technology Demonstration in Industrial Environment: Status of the CLEANKER Pilot Plant. *SSRN Electronic Journal.* https://doi.org/10.2139/SSRN.3817346.

Gardarsdottir, S.O., De Lena, E., Romano, M., Roussanaly, S., Voldsund, M., Pérez-Calvo, J.F., Berstad, D., Fu, C., Anantharaman, R., Sutter, D., Gazzani, M., Mazzotti, M., Cinti, G., 2019. Comparison of technologies for CO 2 capture from cement production—Part 2: Cost analysis. *Energies* 12 (3). https://doi.org/10.3390/en12030542.

Grasa, G.S., Abanades, J.C., 2006. CO2 Capture Capacity of CaO in Long Series of Carbonation/Calcination Cycles. *Industrial and Engineering Chemistry Research* 45 (26), 8846–8851. https://doi.org/10.1021/IE0606946.

Hanak, D.P., Anthony, E.J., Manovic, V., 2015. A review of developments in pilot-plant testing and modelling of calcium looping process for CO2 capture from power generation systems. *Energy and Environmental Science* 8 (8), 2199–2249. https://doi.org/10.1039/c5ee01228g.

Kabir, G., Abubakar, A.I., El-Nafaty, U.A., 2010. Energy audit and conservation opportunities for pyroprocessing unit of a typical dry process cement plant. *Energy* 35 (3), 1237–1243. https://doi.org/10.1016/J.ENERGY.2009.11.003.

Khalifa, S.A., Alsadig, D.Y., 2019. Heat Balance Analysis in Cement Rotary Kiln. *Advances in Applied Sciences* 4 (2), 34–40. https://doi.org/10.11648/J.AAS.20190402.11.

Knowlton, T.M., 2013. Fluidized bed reactor design and scale-up. *Fluidized Bed Technologies for near-Zero Emission Combustion and Gasification* 481–523. https://doi.org/10.1533/9780857098801.2.481.

Lothenbach, B., Matschei, T., Möschner, G., Glasser, F.P., 2008. Thermodynamic modelling of the effect of temperature on the hydration and porosity of Portland cement. *Cement and Concrete Research* 38 (1), 1–18. https://doi.org/10.1016/J.CEMCONRES.2007.08.017.

Marques, L.M., Mota, S.M., Teixeira, P., Pinheiro, C.I.C., Matos, H.A., 2023. Ca-looping process using wastes of marble powders and limestones for CO2 capture from real flue gas in the cement industry. *Journal of CO2 Utilization* 71, 102450. https://doi.org/10.1016/J.JCOU.2023.102450.

Matches' Equipment Cost Estimates. (2014). https://www.matche.com/equipcost/Default.html.

Our World in Data. (2021). https://ourworldindata.org/.

Rodríguez, N., Alonso, M., Abanades, J.C., 2010. Average activity of CaO particles in a calcium looping system. *Chemical Engineering Journal* 156 (2), 388–394. https://doi.org/10.1016/J.CEJ.2009.10.055.

Romano, M.C., 2012. Modeling the carbonator of a Ca-looping process for CO2 capture from power plant flue gas. *Chemical Engineering Science* 69 (1), 257–269. https://doi.org/10.1016/j.ces.2011.10.041.

Romano, M.C., Spinelli, M., Campanari, S., Consonni, S., Marchi, M., Pimpinelli, N., Cinti, G., 2014. The Calcium Looping Process for Low CO2 Emission Cement Plants. *Energy Procedia* 61, 500–503. https://doi.org/10.1016/J.EGYPRO.2014.11.1158.

Spinelli, M., Martínez, I., Romano, M.C., 2018. One-dimensional model of entrained-flow carbonator for CO2 capture in cement kilns by Calcium looping process. *Chemical Engineering Science* 191, 100–114. https://doi.org/10.1016/j.ces.2018.06.051.

Sun, P., Grace, J.R., Lim, C.J., Anthony, E.J., 2008. Determination of intrinsic rate constants of the CaO–CO2 reaction. *Chemical Engineering Science* 63 (1), 47–56. https://doi.org/10.1016/J.CES.2007.08.055.

Verma, Y.K., Mazumdar, B., Ghosh, P., 2020. Thermal energy consumption and its conservation for a cement production unit. *Environmental Engineering Research* 26 (3). https://www.eeer.org/journal/view.php?doi=10.4491/eer.2020.111.

Voldsund, M., Gardarsdottir, S.O., De Lena, E., Pérez-Calvo, J.F., Jamali, A., Berstad, D., Fu, C., Romano, M., Roussanaly, S., Anantharaman, R., Hoppe, H., Sutter, D., Mazzotti, M., Gazzani, M., Cinti, G., Jordal, K., 2019. Comparison of technologies for CO 2 capture from cement production – Part 1 : Technical evaluation – Supplementary Materials. *Energies* 12 (3).